J. Korean Inst. Electr. Electron. Mater. Eng.
Vol. 35, No. 3, pp. 203-214 May 2022
DOI: https://doi.org/10.4313/JKEM.2022.35.3.1
ISSN 1226-7945(Print), 2288-3258(Online)

Academic Progress Report

A Review on Thermoelectric Technology: Conductive Polymer Based Thermoelectric Materials

Dabin Park[1] and Jooheon Kim[1,2,3]

[1] School of Chemical Engineering & Materials Science, Chung-Ang University, Seoul 06974, Korea

[2] Department of Advanced Materials Engineering, Chung-Ang University, Anseong 17546, Korea

[3] Department of Intelligent Energy and Industry, Chung-Ang University, Seoul 06974, Korea

(Received March 6, 2022; Revised March 23, 2022; Accepted March 27, 2022)

Abstract: Thermoelectric (TE) heating and cooling devices, which are able to directly convert thermal energy into electrical energy and vice versa, are effective and have exhibited a potential for energy harvesting. With the increasing consumer demands for various wearable electronics, organic-based TE composite materials offer a promise for the TE devices applications. Conductive polymers are widely used as flexible TE materials replacing inorganic materials due to their flexibility, low thermal conductivity, mechanical flexibility, ease of processing, and low cost. In this review, we briefly introduce the latest research trends in the flexible TE technology and provide a comprehensive summary of specific conductive polymer-based TE material fabrication technologies. We also summarize the manufacture for high-efficiency TE composites through the complexation of a conductive polymer matrix/inorganic TE filler. We believe that this review will inspire further research to improve the TE performance of conductive polymers.

Keywords: Thermoelectric, Conductive polymer, PEDOT:PSS, PANI

1. INTRODUCTION

Society's energy consumption is increasing due to the increase in population and progress in civilization, Accordingly, fossil fuels such as coal and oil, which are energy sources, are gradually being depleted. Therefore, this energy crisis, energy harvesting, which recycles waste energy, has attracted significant attention as an alternative or supplement to the use of fossil fuels. Among them, renewable energy conversion devices, such as piezoelectric devices, fuel cells, solar cells and thermoelectric devices, have been developed [1-8]. Notably, thermoelectric (TE) power generation, involving the generation of electrical energy from waste heat, is effective and has great potential for energy harvesting applications [9-16].

The thermoelectric generator (TEG) using the TE effect is shown in Fig. 1. The n-type and p-type TE materials are bonded and manufactured, and a module in which thermoelectric unit elements are arranged in various shapes and sizes according to the environment of use is manufactured and used.

The performance of TE materials is usually denoted by a dimensionless quantity called the figure of merit (ZT), defined as $ZT=(S^2\cdot\sigma\cdot T)/\kappa$, where S, σ, T, and κ are the Seebeck coefficient, electrical conductivity, absolute temperature, and thermal conductivity, respectively. A high power factor ($PF=S^2\cdot\sigma$) and TE materials with low thermal conductivity are

✉ **Jooheon Kim; jooheonkim@cau.ac.kr**

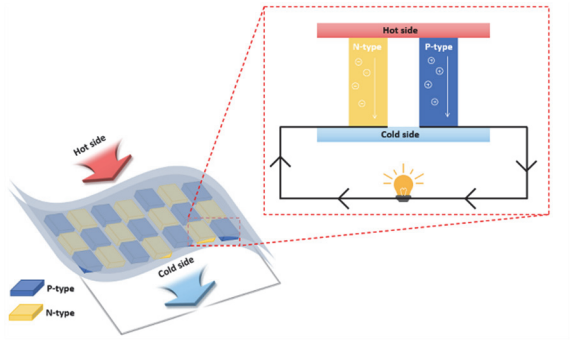

Fig. 1. Schematic of a thermoelectric generator module.

important to high *ZT*. Enhancing the Seebeck coefficient and electrical conductivity are the primary strategies for achieving a high PF value.

Recent, research on TE composite materials has focused on inorganic materials, such as chalcogenide-based materials [17-20], half-Heuslers [21-24] and oxides ($NaCo_2O_4$, Bi_2O_2Se, and $SrTiO_3$ [25-30]) due to their outstanding Seebeck coefficients and electrical conductivity. However, inorganic TE materials are inflexible and do not easily conform a flexible and wearable platform. However, research on organic-inorganic composite materials is being actively conducted to overcome these shortcomings.

Conductive polymers (CPs), such as polyaniline (PANI), polythiophene (PTh) and poly(3,4-ethylenedioxythiophene): poly(4-styrenesulfonate) (PEDOT:PSS) are widely explored in the literature on flexible TE composite materials as replacements for inorganic materials (Fig. 2.) [31-39]. Typically, polymers are electrically insulated and cannot be utilized as TE materials. However, the performance of organic TE materials has drastically improved in the last decade because of the intensive research efforts into CPs, which have the advantages of low cost, good mechanical flexibility, ease of processing, and rich sources [40-44].

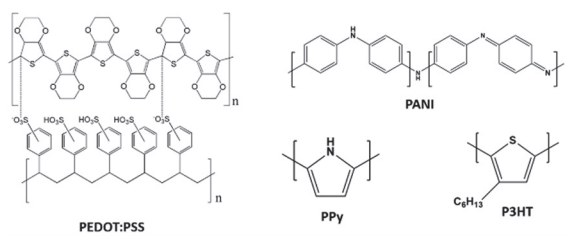

Fig. 2. Schematic of various CPs.

However, pristine CP-based TE materials have critical drawbacks, which primarily in regard to its TE properties, which are worse than those of inorganic TE materials. Additionally, polymer-based TE materials have low thermal stability. A realistic application of these CP-based materials to TE requires operating in the low temperature range, that is, near room temperature.

In this review, we summarize the CP-based thermoelectric composite materials. Chemical synthesis methods and the discovery of CPs are explored. TE composites with PEDOT:PSS and PANI, as a category of CPs, are summarized. Afterward, we provide comprehensive insight into strategies and mechanisms for optimizing the TE performance of CP-based flexible TE composite materials. Specifically, we summarize and present effective CP-based inorganic flexible TE composites that exhibit mechanical flexibility and improved TE performance. Additionally, a variety of recent studies on different composite materials are summarized. A summary of the research status and prospects is presented in the last section, which will serve as a reference for further research.

2. PEDOT:PSS-BASED THERMOELECTRIC MATERIALS

Among the reported CPs, PEDOT:PSS and its composites are critical TE materials because of their outstanding TE PF, which is attributed to a relatively high electrical conductivity,

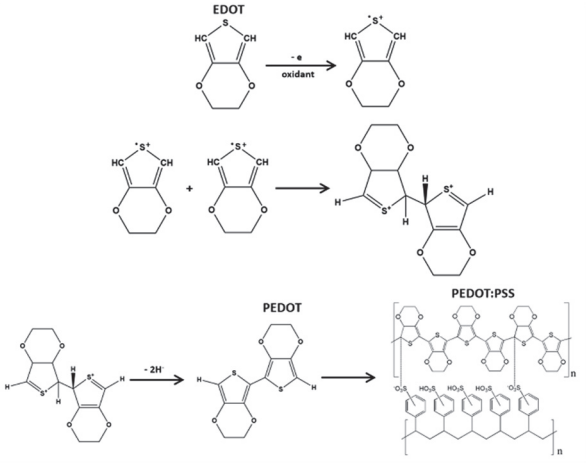

Fig. 3. Polymerization process of PEDOT:PSS.

excellent stability and flexibility. PEDOT is prepared by the oxidation polymerization of EDOT, which involves three main 3 stages. First, EDOT is oxidized to form a cationic radical, which then combines to form a dimer. The dimers are then oxidized and polymerized into PEDOT (Fig. 3). Afterward, being anionic surfactants, PSS counter ions can assist in the dispersion of PEDOT and balancing charge. The as-prepared PEDOT:PSS films have a Seebeck coefficient of ~20 μV/K and an electrical conductivity of less than 1 S/cm (=1 Ω^{-1}·cm), implying a low TE conversion efficiency. This can be improved by doping and secondary treatment. In 2002, Kim et al. reported an enhanced electrical conductivity of ~80 S/cm following the addition of an appropriate amount of organic solvent [45]. Additionally, the dimethyl sulfoxide (DMSO)-treated PEDOT:PSS exhibited an enhanced electrical conductivity and high PF (~620 S/cm and ~33 μW/m·K^2 [46]). Similarly, Luo et al studied a DMSO post-treated PEDOT:PSS thin film with high electrical conductivity (~940 S/cm [47]). However, despite the improvement in performance through doping, pristine PEDOT:PSS exhibits poor TE properties. Therefore, researche on the fabrication of an inorganic/organic composite TE material using inorganic TE fillers, which have good TE properties, is underway.

2.1 PEDOT:PSS/SnSe NS composite film

Chemically exfoliated SnSe nanosheet (NS)/ PEDOT:PSS composite film for TE applications were fabricated [48], and which are shown in Fig. 4. Before its synthesis, the PEDOT:PSS was DMSO post-treated to enhance the electrical conductivity of the PEDOT:PSS matrix. The exfoliated SnSe NSs were fabricated as TE fillers. SnSe ingots were synthesized via a solid state reaction using stoichiometric amounts. The synthesized ingots were ball milled and Li atoms were intercalated into the van der Waals-bonded SnSe interlayers in autoclave. The Li^+ ions intercalated into SnSe and formed Li_xSnSe during reaction. After the lithiated SnSe was exposed to water, the Li^+ ions were solvated to produce LiOH and H_2 gases. The reaction mechanisms are as follows.

$$SnSe + x(LiOH) \rightarrow Li^+{}_x(SnSe)^{-x} + x(OH)^- \quad (1)$$

$$Li_xSnSe + xH_2O \rightarrow SnSe + xLiOH + \frac{x}{2}H_2(\uparrow) \quad (2)$$

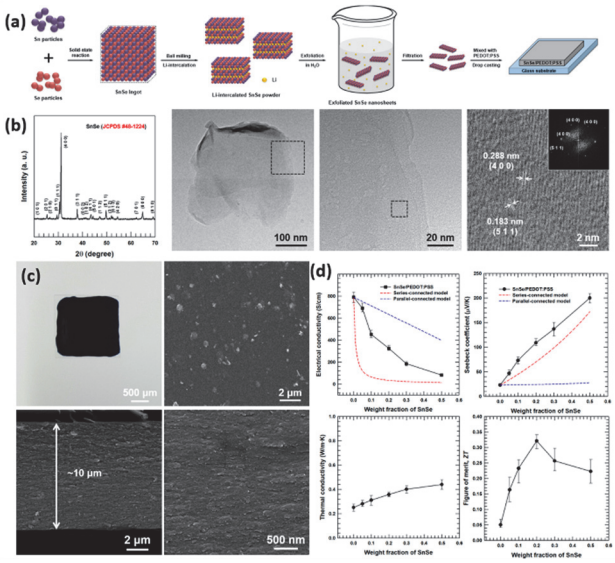

Fig. 4. (a) Schematic of PEDOT:PSS/SnSe NS composite film fabrication process, (b) XRD and TEM images of SnSe NSs, (c) Digital photograph and FE-SEM images of composite film, and (d) TE properties of composite films.

The synthesized SnSe NSs were analyzed via AFM to measure the thickness. The average thickness of the 2D NSs was ~3.4 nm. Afterward, the morphology of the synthesized NSs were analyzed via FE-TEM and XRD analyses, which all verified the the crystal structure of the NSs.

After the successful synthesis of SnSe NSs, they were dispersed in an as-prepared DMSO-treated PEDOT:PSS mixture. The mixture was then drop-casted on a glass substrate to form a composite film ~ 10 μm thick. As clearly seen in the cross-sectional FE-SEM images, the film exhibits a well-filled composite structure without voids. The SnSe NW/PEDOT: PSS composite film was fabricated using different NSs contents (5, 10, 20, 30, and 50 wt%), and the TE properties of composite film were determined for the SnSe NS contents. With an increase in SnSe NS contentss, the Seebeck coefficient of the composite film exhibited an increasing trend. In contrast, the electrical conductivity of the composite film reduced with increasing NS content. This trend is further analyzed via Hall-measurements.

$$\sigma = n \cdot e \cdot \mu$$
$$S = \frac{8 \cdot \pi^2 \cdot {k_B}^2}{3 \cdot e \cdot h^2} \cdot m^* \cdot T \cdot \left(\frac{\pi}{3 \cdot n}\right)^{\frac{2}{3}} \quad (3)$$

where n, e, μ, k_B, h, and m^* are the carrier concentration,

electron charge, carrier mobility, Boltzmann constant, Planck constant, and effective mass of the carrier, respectively. As the NS content increased, n exhibited an increasing trend, and μ decreased. After measuring the Seebeck coefficient and electrical conductivity, the PF was calcluated; the highest PF corresponded to 20 wt% NS content. Finally, the thermal conductivity and ZT of the composite films were measured. The highest ZT (~0.32 at room temperature) of the SnSe NW/PEDOT: PSS composite film corresponded to a 20 wt% SnSe NS contents.

2.2 PEDOT-coated $SnSe_{0.97}Te_{0.03}$ NS/PEDOT:PSS composite film

Tin-chalcogenide TE filler/conductive polymer flexible composite films were also fabricated [49]. The aim of this study is to enhance TE performance by combining $SnSe_{0.07}Te_{0.03}$ NSs with a PEDOT:PSS matrix. The exfoliated NSs from the bulk $SnSe_{0.07}Te_{0.03}$ sample exhibit better TE properties than the bulk structure. The $SnSe_{0.07}Te_{0.03}$ NSs were fabricated under hydrothermal conditions, including Li intercalation and exfoliation. To increase the compatibility between the synthesized NS and the PEDOT:PSS matrix, the surface of the NSs were finely coated with PEDOT. Further, dodecylbenzenesulfonic acid was used as both a surfactant for NS colloidal states of and a doping agent for PEDOT polymerization.

The morphology of $SnSe_{0.07}Te_{0.03}$ NS and PEDOT-coated $SnSe_{0.07}Te_{0.03}$ NSs were confirmed via FE-TEM imaging, and the presence of a PEDOT-coating layer was confirmed [Fig. 5(a) and (c)]. Afterward, the XRD and XPS analyses of the crystal structure and binding structure of the $SnSe_{0.07}Te_{0.03}$ NS and PEDOT-coated $SnSe_{0.07}Te_{0.03}$ NS were conducted [Fig. 5(b)]. These confirmed that the morphology of the NS composite did not significantly collapse during the coating process and that the surface of $SnSe_{0.07}Te_{0.03}$ NS was well coated with PEDOT.

$SnSe_{0.07}Te_{0.03}$ NS and PEDOT-coated $SnSe_{0.07}Te_{0.03}$ NS were dispersed with PEDOT:PSS solutions and drop-casted to fabricate the NS/PEDOT:PSS composite film; both composite films exhibited high flexibility. The FE-SEM was conducted to compare the morphology of the two composite films and demonstrate the effect of PEDOT nanocoating on the morphology of the composite. The PEDOT-coated

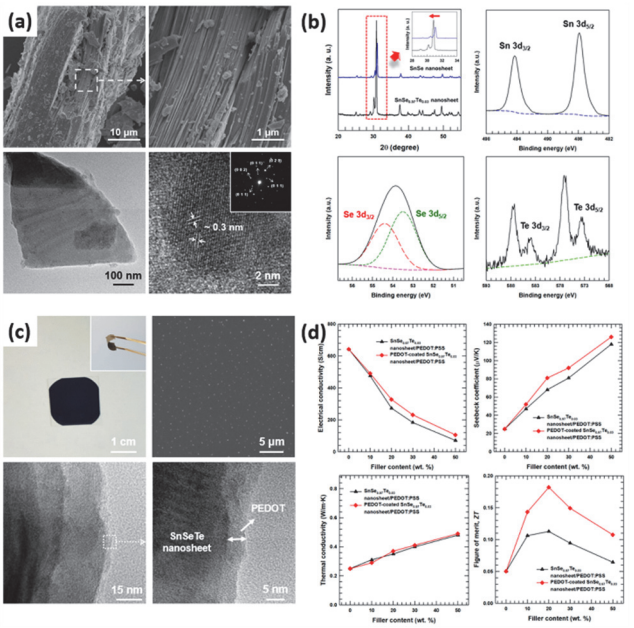

Fig. 5. (a) FE-SEM and FE-TEM images of SnSeTe composite, (b) SEM, and FE-TEM images of PEDOT-coated SnSeTe composite film, and (d) TE properties of PEDOT:PSS-SnSeTe composite films.

$SnSe_{0.07}Te_{0.03}$ NSs were evenly distributed in the composite and differ from the composite with pristine $SnSe_{0.07}Te_{0.03}$ NSs. After investigating the effect of the PEDOT nano-coating on the NS morphology in the PEDOT:PSS matrix, the TE performance of PEDOT-coated $SnSe_{0.07}Te_{0.03}$ NS/PEDOT: PSS flexible composite film as function of the NW content was investigated. The electrical conductivity of the composite film exhibited a decreasing trend with increasing filler content, and the Seebeck coefficient increased as the content increased. Overall, composite with PEDOT-coated $SnSe_{0.07}Te_{0.03}$ NS fillers exhibited a higher Seebeck coefficient and electrical conductivity than the pristine $SnSe_{0.07}Te_{0.03}$ NS/PEDOT:PSS composite film. The calculated ZT value reflecting these trends. The PEDOT:PSS-coated $SnSe_{0.07}Te_{0.03}$ NS/PEDOT: PSS composite film had the highest ZT (0.18 at room temperature) at 20 wt% PEDOT:PSS-coated $SnSe_{0.07}Te_{0.03}$ NS, which is ~61% higher than that of the $SnSe_{0.07}Te_{0.03}$ NS/PEDOT:PSS composite film with 20 wt% $SnSe_{0.07}Te_{0.03}$ NS.

2.3 PEDOT-coated Se NW/MWCNT composite film for flexible TE application

As describe above, to improve the compatibility of the composite thermoelectric filler, the surface of TE filler was coated with CP. The composite was further complexed with MWCNTs to achieve outstanding TE properties [50]. Herein, a strategy to synthesize an inorganic/organic composite from PEDOT:PSS-coated Se NW through a simple solution mixing method is reported, and the enhanced TE properties are achieved. Se NW, which has a wire-liked structure in the form of a 1D nanostructure, was synthesized through a solution mixing process with a Se precursor solution. After mixing an SeO_2, L-ascorbic acid, β-cyclodextrin, and PEDOT:PSS solution, an Se nanoparticle was formed via the following reaction.

$$SeO_2 + 2C_6H_8O_6 \rightarrow Se + 2C_6H_6O_6 + 2H_2O \quad (4)$$

Notably, SeO_2 was reduced by the reaction of ascorbic acid. In forming the Se nanoparticle, the mixed PEDOT:PSS in the solution combined with the nanoparticle surface, to finally produce the PEDOT:PSS-coated Se nanoparticles [Fig. 6(a)]. The synthesized PEDOT:PSS-coated Se nanoparticles were stored in an ethanol solution, and then grown in a preferential orientation of (100). The result was a 1D wire-like shape, and the generation of PEDOT:PSS-coated Se NWs.

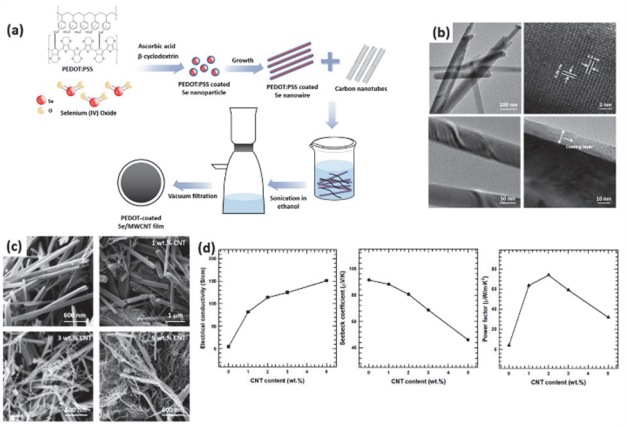

Fig. 6. (a) Schematic of PEDOT:PSS/Se NW/MWCNT composite film fabrication process, (b) TEM images of Ag2Se and PEDOT:PSS-Se composite, (c) FE-SEM images of PEDOT:PSS-Se/MWCNT composite with various MWCNT contents, and (d) TE properties of composite films.

After synthesis, the morphology and crystal structure of the pristine Se NWs and PEDOT:PSS-coated Se NWs were analyzed via FE-TEM and XRD. In the FE-TEM images of pristine NWs, the lattice fringe of Se NWs were clearly visible, and the crystal structure of the NWs were further confirmed by the XRD analysis. Additionally, the PEDOT:PSS coating layer markedly visible in the FE-TEM images of PEDOT:PSS-coated Se NWs [Fig. 6(b)]. After confirming successful synthesis, the TE properties of PEDOT:PSS-coated Se NW were evaluated; the PF of the composite was ~4.1 $\mu W/m \cdot K^2$. To further improve the of TE performance of the PEDOT:PSS-coated Se NW composite, a small amount of CNTs with high electrical conductivity was introduced into the composite film. Individual CNT particles distributed within the composite film act as electrically connected pathways, thus promoting high electrical conductivity. Thereafter, the TE properties were evaluated by adjusting the ratio of CNTs. As the CNT amount increased, the Seebeck coefficient decreased, and the electrical conductivity increased. The highest PF was ~58.91 $\mu W/m \cdot K^2$ at room temperature and 2 wt% CNTs. Moreover, the PF of the composite film decreased by only 7.1% after 1,000 bending cycles. Therefore, the composite film exhibits high TE performance with outstanding durability to bending.

2.4 PEDOT:PSS-coated Ag_2Se NW/PEDOT:PSS flexible composite film and power generator

An additional CP-coated chalcogenide-based NW was fabricated, and the results of the fabrication of the flexible TE composite film are herein reported [51]. PEDOT:PSS-coated Ag_2Se NW were synthesized via simple solution mixing method. As in the previous experiments, PEDOT:PSS-coated Se NWs were formed, and the synthesized NWs were reacted with an Ag precursor solution to form PEDOT:PSS-coated Ag_2Se NWs. The reactions during for the fabrication of Ag_2Se NWs is summarized below:

$$2Ag^+ + C_6H_8O_6 \rightarrow 2Ag + C_6H_6O_6 + 2H^+$$
$$2Ag + Se \rightarrow Ag_2Se \quad (5)$$

Ag^+ is first reduced by the ascorbic acid to form Ag. The as-synthesized PEDOT:PSS-coated Se NW reacts with Ag and

produces the PEDOT:PSS-coated Ag_2Se NWs. Regarding this synthesis, it was confirmed through FE-TEM analysis that the one-dimensional wire-like nanostructure was maintaining without collapsing. In addition, the nano-coated PEDOT:PSS layer on the surface of Ag_2Se NW was confirmed by the FE-TEM images. The TE properties of the PEDOT:PSS-coated Ag_2Se NW are measured, and the results are shown in Fig. 7. After confirming the TE properties of the composites, flexible TE composite films were prepared by compounding these PEDOT:PSS-coated Ag_2Se NWs into a PEDOT:PSS polymer matrix using them as TE fillers. The as-synthesized PEDOT:PSS-coated Ag_2Se NWs were dispersed in a PEDOT:PSS solution and sonicated for the appropriate minutes. This mixture was then drop-casted and dried to produce the composite film a black square with a length of 18 mm and outstanding flexible characteristics. The TE properties of the flexible composite film were evaluated under different PEDOT:PSS-coated Ag_2Se NW contents. The 50 wt% of TE filler composite film exhibited the highest PF of ~327.15 $\mu W/m \cdot K^2$ at room temperature. Additionally, the bending test revealed its outstanding durability after 1,000 bending cycle.

A flexible TE prototype generator was assembled using the prepared flexible TE composite films. The composite films were cut into strips (18 × 6 mm). The five strips were connected to the polyimide flexible film using paste and joined to the Cu wire and Ag paste. The simple TE device made using the composite film is shown in Fig. 7(d). The open-circuit voltage and output power were measured using a homemade device; the measured open-circuit voltage was 7.6 mV with a temperature difference of 20 K. A simple circuit with a thermocouple and voltage measurement was designed to measure the output properties of the device. The maximum output power of the device was 353.92 NW for a temperature difference of 30 K, and the load resistance was 91.6 Ω.

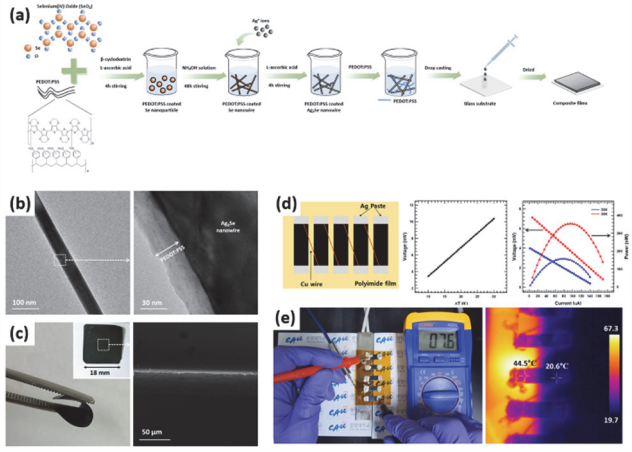

Fig. 7. (a) Schematic of PEDOT:PSS/Ag2Se NW composite film fabrication process, (b) TEM images of PEDOT:PSS-coated Ag2Se NW, (c) digital photograph and SEM images of PEDOT:PSS-coated Ag2Se composite films, (d) schematic of TE device and device properties of fabricated TE device, and (e) TE properties of composite films.

3. PANI-BASED THERMOELECTRIC MATERIALS

PANI, a promising CP, has been extensively studied because of its facile synthesis and interesting properties, such as flexibility, chemical stability and solution processability. Moreover, it can be n- or p-doped [52-54]. That is, the main charge carrier type of PANI can be controlled through pH adjustment of the dopant or grafting of inorganic/organic parts in the polymer chains. Additionally, PANI synthesis can be simply conducted by electrochemically and chemically, and the morphologies and properties depend on the synthesis method. This is attributable to the electrical conductivity of PANI being dependent on the oxidation state; PANI has three different oxidation states and acid/base doping response: entirely reduced leucomeraldin or LEB, partial-oxidized

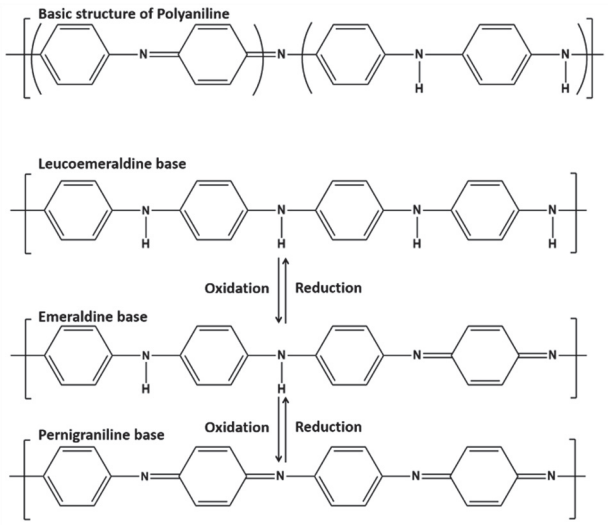

Fig. 8. Basic PANI in three dissimilar types.

emerald or EB, and entirely oxidized pernigraniline or PAB (Fig. 8) [55]. Li et al. studied the change in TE properties according to the HCl doping concentration [ref]. The PANI composite exhibits the highest ZT with ~3 × 10^{-4} at 473 K under HCl doping [56]. Camphorsulphonic (CSA)-doped PANI with enhanced ZT (2.17 at 17 K) was achieved by Nath et al [57]. Polymer chain crosslinking can enhance the TE properties of PANI. In the aforementioned study, the mobility and conductivity increased by approximately ~25% compared to linear PANI. This phenomenon improved charge transport and crystallinity.

3.1 PANI/SnS nanosheet composite

A promising method for achieving outstanding TE performance by fabricating inorganic/organic hybrid composites consisting of SnS NS and PANI has been reported [58]. SnS is a potentially efficient TE filler material for enhancing the TE properties of CPs due to its high Seebeck coefficient at room temperature. The PANI used in this study is CSA-doped to enhance its TE properties in the pristine state. After fabrication of the CSA-PANI, different amounts of SnS NSs were intercalated into the hybrid composites. SnS NSs were chemically exfoliated from a bulk SnS ingot, which was pulverized, intercalated with Li, and exfoliated to form the NSs. During intercalation, the weak bonding of Sn-S along the a-axis the SnS was peeled off after exposing the SnS powder intercalated with Li to water.

The fabricated NSs were analyzed via the XRD and XPS to characterize the composite sample. The crystal structure of SnS NSs was confirmed via XRD. The XPS survey spectrum of the NSs clearly shows the binding energies of the Sn 3d and S 2p core level spectrum of SnS composites [Fig. 9(a)]. The nanostructure of fabricated SnS sample was then characterized via FE-SEM and FE-TEM. The layered internal structure of the synthesized bulk SnS sample was confirmed by the FE-SEM images [Fig. 9(b)]. Afterward, the FE-TEM analysis of the structure of the exfoliated NSs was conducted, and the thin sheet structure was confirmed.

The fabricated SnS NS were then mixed with a PANI solution and stirred overnight. The mixture was then washed and dried in an oven. Finally, the composites were hot-pressed, and the morphology of the pressed samples was characterized via cross-sectional FE-SEM. The average thickness of

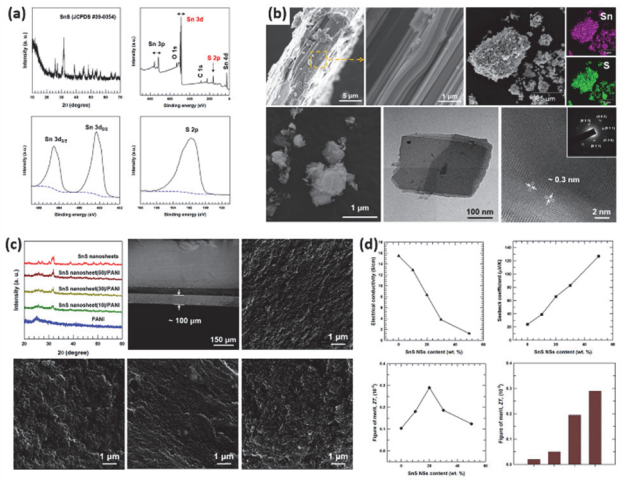

Fig. 9. (a) XRD and XPS of SnS NS composites, (b) FE-SEM, EDS and FE-TEM images of SnS NS composites, (c) XRD and FE-SEM images of PANI-SnS composites, and (d) TE properties of PANI-SnS composites.

composite sample was ~ 100 μm. The hybrid composites were prepared with different NS contents (10, 20, 30, and 50 wt%), and effect of the SnS NSs composition on the TE properties was determined. Because the Seebeck coefficient of SnS is higher than that of PANI, that of the composite exhibited an increasing trend with an increase in NS filler. In contrast, the electrical conductivity of the composite sample exhibited a slight decreasing trend. Finally, the hybrid composite with 20 wt% SnS NSs exhibited the highest ZT of ~0.003 at room temperature, which is higher than that of other PANI-based composites, such as CNT/PANI, Ag particles/PANI, and graphene NS/PANI [Fig. 9(d)] [59-61].

3.2 PANI/SnS nanosheet composite

A chalcogenide-based inorganic/organic hybrid composite fabricated with PANI and SnS NSs was synthesized and its outstanding TE properties were reported (Fig. 10) [62]. The hybrid TE material comprised porous SnS NS and PANI. The SnS NSs had a porous structure with numerous nanosized pores. SnS NSs were first fabricated with via Li-intercalation and exfoliation of the SnS sample. The as-synthesized SnS NSs were then chemically reacted with tartaric acid to introduce numerous nano sized pores into the NS structure. An aqueous solution containing SnS NS and tartaric acid was hydrothermally treated at a high temperature in the presence

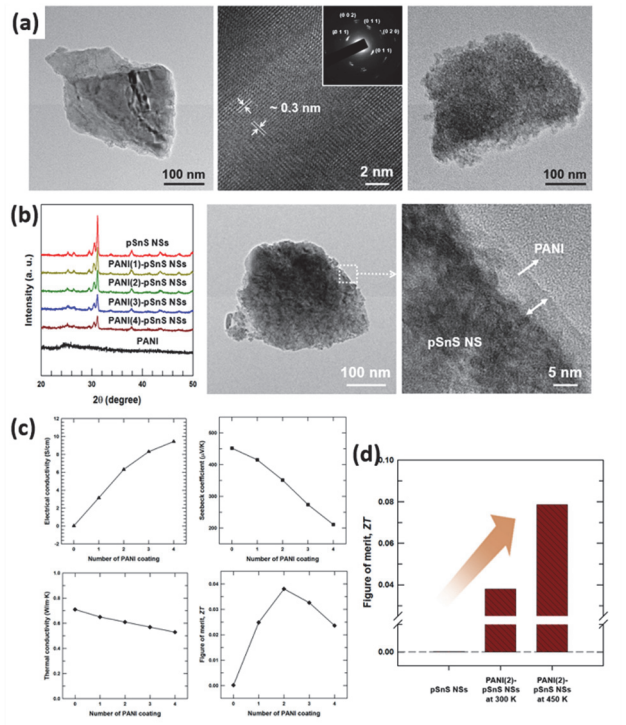

Fig. 10. (a) FE-TEM images of pSnS NSs, (b) XRD and FE-TEM images of PANI-pSnS composite, (c) TE properties of PANI-pSnS composites, and (d) ZT values of the PANI(2)-pSnS NSs at 450 K compared to those of pristine pSnS Ns and the PANI(2)-pSnS NS at 300 K.

of O_2. The reaction mechanism is as follows:

$$C_4H_6O_6 \text{ (tartaric acid)} + SnS \rightarrow Sn^{2+}(C_4H_4O_6)^{2-} + S^{2-} + 2H^+$$

$$S^{2-} + 0.5O_2 + H_2O \rightarrow S + 2OH^- \quad (6)$$

First, Sn^{2+} ions in the SnS NS were attacked by the tartaric acid, causing their depletion. Meanwhile, S^{2-} ions in the surface of NS surface oxidized to S^0 by O_2. Therefore, SnS with a porous structure was obtained through a partial-solution phase strapping of Sn^{2+} ions with tartaric acid and O_2. FE-TEM analysis was conducted to determine the morphology of the synthesized SnS NSs and porous SnS NSs, the nano sized porous structure of the treated NSs. After fabrication, the porous NSs were dispersed in solution to form PANI-coated NSs. In this polymerization reaction, dodecylbenzenesulfonic acid (DBSA) is used as both a surfactant for the formation of colloidal NSs and a doping agent.

PANI-coated porous SnS NSs (P-SnS NSs) were synthesized with different PANI contents. With increasing PANI content, the XRD peaks indicating SnS crystal structure were decreased. The PANI coating layer of P-SnS NSs was confirmed by the FE-TEM images, and the average coating layer was ~5 nm. The changes in the TE properties with the number of PANI coating was measured. As the number of PANI coatings increased, the electrical conductivity of the P-SnS NS increased and the Seebeck coefficient of the composite exhibited a decreasing trend. These trends are further evinced in the electrical transport data corresponding to changes in carrier mobility and concentration. The carrier concentration rapidly increased with additional the PANI coatings (~10^{18} → ~10^{21}), and the Seebeck coefficient decreased with a change in the carrier concentration. The highest ZT of the P-SnS NS composite is ~0.0038 at room temperature and with two PANI coatings [P(2)-SnS NS]. Additionally, the temperature-dependent ZT of P(2)-SnS NSs was measured; the highest value was ~0.078 at 450 K, which is 458 times higher than that of the pristine P-SnS NSs.

3.3 PANI-coated SnSeS nanosheet/PVDF flexible composite film

An inorganic/organic composite TE film was fabricated using high-durability PANI, and its outstanding TE properties were reported [63]. In this study, a PVDF-based flexible TE composite film was fabricated via solution-based mixing and utilizing a drop-casting method. PANI-coated exfoliated SnSe NSs were chosen as the TE filler. SnSeS NSs were fabricated following the same procedure in previous studies. Afterward, as-synthesized SnSeS NSs were utilized in the polymerization of aniline, during which DBSA was used as a surfactant to form the SnSeS NS colloidal particles and as a doping agent. The high-magnification of FE-TEM images confirmed the crystal structure of the SnSeS NSs and the PANI coating layer in the PANI-SnSeS (Fig. 11). The PANI-SnSeS composites were fabricated under different PANI coating cycles, and TGA was performed to measure the amount of PANI corresponding to the number of coatings. Further, the TE properties of PANI-SnSeS composite according to PANI coating number were evaluated.

The PANI-SnSeS formed under two PANI coating cycles [PANI(2)-SnSeS] exhibited the highest PF of ~250 μW/m·K^2 at room temperature; accordingly, PANI(2)-SnSeS was

selected as the TE filler. The electrical conductivity of the PANI-SnSeS composite increased with an increasing number of coating cycles. The deposited PANI coating layer formed a conductive network between the PANI and SnSeS NS structure. However, the Seebeck coefficient slightly decreased following the addition of a PANI coating.

The fabricated PANI(2)-SnSeS and polyvinylidende fluoride (PVDF) with different ratios were mixed into the DMF solution and sonicated. Afterward, the PANI-SnSeS/PVDF composite was drop-casted to fabricate the composite films. The fabricated composite film exhibits flexible properties and curved shapes, and the morphology of the composite film is further investigated via the FE-SEM analysis. The good-distibution of PANI-SnSeS fillers in the PVDF matrix was revealed by the FE-SEM images of composite film.

The composite film was fabricated using different TE filler to PVDF ratios (PANI-SnSeS:PVDF = 1:1, 2:1, and 3:1). To confirm the durability of the composite sample, the TE properties changes corresponding to different PVDF amount during a bending cycle were measured. The PANI-SnSeS/PVDF composite film with a PANI-SnSeS ratio of 3:1 initially exhibited the highest PF. However, this was rapidly decreased after 1,000 bending cycles. Thus, the PANI-SnSeS composite film with an NS/PVDF ratio of 2:1 had better TE properties and outstanding durability after 1,000 bending cycles. These inorganic/organic hybrid composite films exhibit a higher TE PF than other PANI-based composite [64-67].

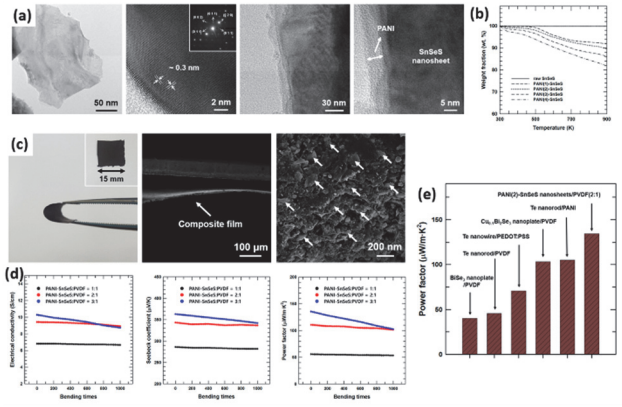

Fig. 11. (a) FE-TEM images of SnSeS NSs, (b) TGA curve of PANI-SnSeS NSs, (c) digital photograph and FE-SEM images of PANI-SnSeS NSs composite film, (d) TE properties of PANI-SnSeS/PVDF film as a function of bending cycle, and (e) PF value of the sample at 300 K compared to the previously reported materials.

3.4 PANI-coated Ag_2Se nanowire/PVDF flexible composite film and thermoelectric device

In this study, PANI-coated silver selenide/ polyvinylidene fluoride (PANI-Ag_2Se/PVDF) composite film was synthesized through simple solution mixing and drop-casting method. In addition, a simple TE device was constructed using the prepared film. TE device made using this film is reported [68]. Ag_2Se is an N-type semiconductor material with a high Seebeck coefficient and electrical conductivity. Therefore, it is widely used as a TE material. The Ag_2Se used in this study was synthesized in the form of NWs with one-dimensional nanostructure. The Se NWs were first synthesized by the reduction of SeO_2; this Se NW reacted with Ag to form Ag_2Se NWs. The surface of the NWs was then coated with PANI using a DBSA solution mixing method. Through this polymerization process, PANI was successfully coated on the NW surface, and CSA-doping was then performed to enhance the electrical conductivity of the PANI-Ag_2Se composite. The wire-like structure and PANI coating layer in thePANI-Ag_2Se composite was confirmed, as shown in the FE-TEM images in

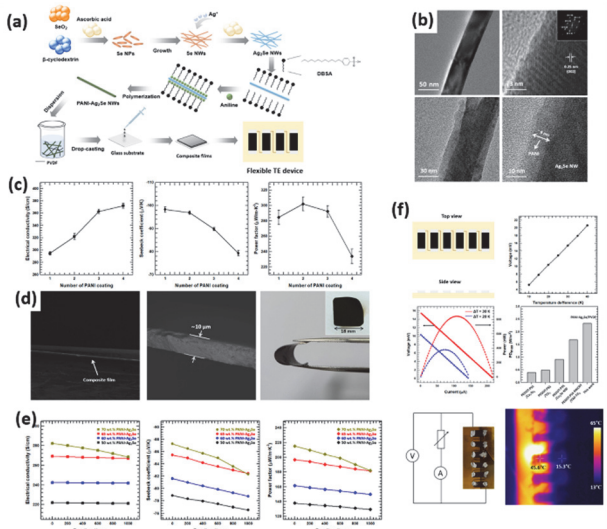

Fig. 12. (a) Schematic of PANI-Ag2Se NW/PVDF composite film fabrication process, (b) TEM images of PANI Ag2Se, (c) Te properties of PANI-Ag2Se, (d) FE-SEM and digital photograph PANI-Ag2Se/PVDF composite film, (e) TE properties of PANI-Ag2Se/PVDF film as a function of bending cycle (TE properties of composite films), and (f) Schematic of TE device and device properties of fabricated TE device.

Fig. 12(b). To investigate the effect of the PANI coating on the TE properties, the electrical conductivity, Seebeck coefficient, and PF were measured for different PANI coating cycles. The PANI-Ag_2Se composite with a double coated [PANI(2)-Ag_2Se] exhibited the highest PF of ~301 μW/m·K^2, and was selected as for use as a high-performance TE filler. The PANI(2)-Ag_2Se were dispersed in the PVDF matrix and drop-casted to form square composite film of ~18 mm length with an average film thickness of ~10 μm. To confirm the flexibility and durability of composite film, bending test were conducted. The PANI(2)-Ag_2Se/PVDF composite film of 70 wt% PANI-Ag_2Se exhibited the highest PF. However, the TE properties of the composite film with 70 wt% filler tended to rapidly decrease after 1,000 bending cycle.

A simple TE device consisting of a PANI(2)-Ag_2Se/PVDF composite with 65 wt% PANI(2)-Ag_2Se was assembled to apply to evaluate its practical application. The manufactured TE device consisted of six composite film strips, and each films connected to the Cu wire and Ag paste. A simple sketch and digital photograph of the TE device was illustrated in Fig. 12(f). The output voltage and output power of TE devices were measured at two different temperatures (20 and 30 K), and the highest output power was 835.8 nW. Finally, the maximum power density (PD_{max}) was measured and compared with that of other TE devices: [69-72], the PD_{max} of the fabricated device was ~2.33 W/m^2.

4. CONCLUSION

In this review, we provide a brief overview of the progress in the development of polymer-based TE composites with enhanced TE properties. CP-based TE materials have unique advantages over inorganic TE materials, such as flexibility, ease of processing, and low cost. However, the pristine CP-based TE materials generally exhibit inferior lower TE properties to inorganic TE materials. The studies herein reviewed suggest new strategies for the applications of polymer-based, high-efficiency TE composites.

Among the CPs, the PEDOT and PANI-based materials especially have attractive attention. The improved TE properties of CPs are through various composition methods. In brief, it was possible to achieve good TE properties while maintaining the unique properties of CPs fabricating the composite with inorganic TE fillers having outstanding TE properties.

Additionally, we discuss the factors influencing the TE properties of organic/inorganic composite TE materials and review strategies for improving TE performance, as well as recent advances in research on TE transport in polymers. We present several prospects for future studies in developing high-performance CP-based materials and devices, and there are summarized below:

(i) For the traditional TE composites mainly include inorganic based TE materials. Chalcogenide- based inorganic TE materials such as Bi_2Te_3, Ag_2Se and SnSe are commonly used as TE materials. However, traditional inorganic TE materials rigid, toxic, and expensive. CPs have the advantages of low thermal conductivity, low cost, nontoxicity and flexibility. Organic-Inoranic TE composites, which combine the advantages of the low thermal conductivity of CPs and high Seebeck coefficient of inorganic TE materials, organic-inorganic TE composites have the characteristics of organic mateirlas and exhibit large TE properties than pure CPs.

(ii) Fabrication of organic-inorganic composite TE composite materials is advantageous in terms of flexibility as well as outstanding TE properties. In the recent studies mentioned in this review, the fabrication of CP-based flexible TE composite films was reported. This assembled TE device offers higher output performance due to the TE composite's high ZT value. This demonstrates the feasibility of converting thermal energy into electricity using organic semiconductor-based TE composites.

(iii) The discovery of new CPs with higher carrier mobilities in the future may increase the development of CP-based TE materials. Moreover, new nanofillers with higher Seebeck coefficient or larger electrical conductivity are likely to provide more contributions to improving the TE properties of organic-inorganic TE composites. This higher energy conversion efficiency of flexible TE composite materials have a wide range of applications, such as power generators to harvest thermal energy and power electronics.

ORCID
Jooheon Kim https://orcid.org/0000-0002-6644-7791

ACKNOWLEDGEMENT

This work was supported by the MSIT (Ministry of Science and ICT), Korea, under the ITRC (Information Technology Research Center) support program (IITP-2021-2020-0-01655) supervised by the IITP (Institute of Information & Communications Technology Planning & Evaluation).

REFERENCES

[1] N. Sezer and M. Koç, *Nano Energy*, **80**, 105567 (2021). [DOI: https://doi.org/10.1016/j.nanoen.2020.105567]

[2] H. C. Song, S. W. Kim, H. S. Kim, D. G. Lee, C. Y. Kang, and S. Nahm, *Adv. Mater*., **32**, 2002208 (2020). [DOI: https://doi.org/10.1002/adma.202002208].

[3] Y. Guo, J. Wang, S. Shinde, X. Wang, Y. Li, Y. Dai, J. Ren, P. Zhang, and X. Liu, *RSC Adv*., **10**, 25874 (2020). [DOI: https://doi.org/10.1039/D0RA05234E]

[4] F. Ma, C. Fu, J. Yang, and Q. Yang, *J. Energy Eng*., **146**, 04019034 (2020). [DOI: https://doi.org/10.1061/(ASCE)EY.1943-7897.0000640]

[5] Y. Liu, N. Sun, J. Liu, Z. Wen, X. Sun, S. T. Lee, and B. Sun, *ACS Nano*, **12**, 2893 (2018). [DOI: https://doi.org/10.1021/acsnano.8b00416]

[6] H. Sharma, A. Haque, and Z. A. Jaffery, *J. Renewable Sustainable Energy*, **10**, 023704 (2018). [DOI: https://doi.org/10.1063/1.5006619]

[7] X. L. Shi, J. Zou, and Z. G. Chen, *Chem. Rev*., **120**, 7399 (2020). [DOI: https://doi.org/10.1021/acs.chemrev.0c00026]

[8] Y. Wang, L. Yang, X. L. Shi, X. Shi, L. Chen, M. S. Dargusch, J. Zou, and Z. G. Chen, *Adv. Mater*., **31**, 1807916 (2019). [DOI: https://doi.org/10.1002/adma.201807916]

[9] G. J. Snyder and E. S. Toberer, *Nat. Mater.*, **7**, 105 (2008). [DOI: https://doi.org/10.1038/nmat2090]

[10] M. Zebarjadi, K. Esfarjani, M. S. Dresselhaus, Z. F. Ren, and G. Chen, *Energy Environ. Sci*., **5**, 5147 (2012). [DOI: https://doi.org/10.1039/C1EE02497C]

[11] Q. Zhang, Y. Sun, W. Xu, and D. Zhu, *Adv. Mater*., **26**, 6829 (2014). [DOI: https://doi.org/10.1002/adma.201305371]

[12] K. Biswas, J. He, I. D. Blum, C. I. Wu, T. P. Hogan, D. N. Seidman, V. P. Dravid, and M. G. Kanatzidis, *Nature*, **489**, 414 (2012). [DOI: https://doi.org/10.1038/nature11439]

[13] J. Y. Oh, J. H. Lee, S. W. Han, S. S. Chae, E. J. Bae, Y. H. Kang, W. J. Choi, S. Y. Cho, J. O. Lee, H. K. Baik, and T. I. Lee, *Energy Environ. Sci*., **9**, 1696 (2016). [DOI: https://doi.org/10.1039/C5EE03813H]

[14] P. Nan, A. Li, L. Cheng, K. Wu, Z. Liang, F. Lin, C. Fu, T. Zhu, and B. Ge, *Mater. Today Phys.*, **21**, 100524 (2021). [DOI: https://doi.org/10.1016/j.mtphys.2021.100524]

[15] S. Han, Z. Zhou, C. Sheng, R. Hu, H. Yuan, Q. Tang, and H. Liu, *Mater. Today Phys*., **21**, 100560 (2021). [DOI: https://doi.org/10.1016/j.mtphys.2021.100560]

[16] M. Guo, J. Zhu, F. Guo, Q. Zhang, W. Cai, and J. Sui, *Mater. Today Phys*., **15**, 100270 (2020). [DOI: https://doi.org/10.1016/j.mtphys.2020.100270]

[17] D. Park, H. Ju, and J. Kim, *J. Alloys Compd.*, **748**, 305 (2018). [DOI: https://doi.org/10.1016/j.jallcom.2018.03.176]

[18] H. Ju, M. Kim, and J. Kim, *Chem. Eng. J*., **275**, 102 (2015). [DOI: https://doi.org/10.1016/j.cej.2015.04.042]

[19] H. Ju and J. Kim, *Dalton Trans.*, **44**, 11755 (2015). [DOI: https://doi.org/10.1039/C5DT00897B]

[20] D. Park, H. Ju, and J. Kim, *Ceram. Int.*, **43**, 11156 (2017). [DOI: https://doi.org/10.1016/j.ceramint.2017.05.163]

[21] C. Fu, S. Bai, Y. Liu, Y. Tang, L. Chen, X. Zhao, and T. Zhu, *Nat. Commun.*, **6**, 8144 (2015). [DOI: https://doi.org/10.1038/ncomms9144]

[22] L. Huang, Q. Zhang, B. Yuan, X. Lai, X. Yan, and Z. Ren, *Mater. Res. Bull*., **76**, 107 (2016). [DOI: https://doi.org/10.1016/j.materresbull.2015.11.032]

[23] T. Zhu, C. Fu, H. Xie, Y. Liu, and X. Zhao, *Adv. Energy Mater*., **5**, 1500588 (2015). [DOI: https://doi.org/10.1002/aenm.201500588]

[24] S. W. Kim, Y. Kimura, and Y. Mishima, *Intermetallics*, **15**, 349 (2007). [DOI: https://doi.org/10.1016/j.intermet.2006.08.008]

[25] T. Liu, C. Wang, J. Hou, C. Zhang, H. Chen, H. He, N. Wang, H. Wu, and G. Cao, *Small*, **12**, 5146 (2016). [DOI: https://doi.org/10.1002/smll.201601616]

[26] I. Terasaki, *Phys. B*, **328**, 63 (2003). [DOI: https://doi.org/10.1016/S0921-4526(02)01810-0]

[27] B. Zhan, Y. Liu, X. Tan, J. L. Lan, Y. H. Lin, and C. W. Nan, *J. Am. Ceram. Soc*., **98**, 2465 (2015). [DOI: https://doi.org/10.1111/jace.13619]

[28] M. Kim, D. Park, and J. Kim, *J. Alloys Compd*., **851**, 156905 (2021). [DOI: https://doi.org/10.1016/j.jallcom.2020.156905]

[29] D. Park, H. Ju, and J. Kim, *Ceram. Int*., **45**, 16969 (2019). [DOI: https://doi.org/10.1016/j.ceramint.2019.05.245]

[30] D. Park, H. Ju, and J. Kim, *Polymers*, **12**, 777 (2020). [DOI: https://doi.org/10.3390/polym12040777]

[31] Q. Yao, Q. Wang, L. Wang, and L. Chen, *Energy Environ. Sci*., **7**, 3801 (2014). [DOI: https://doi.org/10.1039/C4EE01905A]

[32] J. Chen, L. Wang, X. Gui, Z. Lin, X. Ke, F. Hao, Y. Li, Y. Jiang, Y. Wu, X. Shi, and L. Chen, *Carbon*, **114**, 1 (2017). [DOI: https://doi.org/10.1016/j.carbon.2016.11.074]

[33] H. J. Lee, G. Anoop, H. J. Lee, C. Kim, J. W. Park, J. Choi, H. Kim, Y. J. Kim, E. Lee, S. G. Lee, Y. M. Kim, J. H. Lee, and J. Y. Jo, *Energy Environ. Sci*., **9**, 2806 (2016). [DOI: https://doi.org/10.1039/C5EE03063C]

[34] Z. Golsanamlou, S. I. Vishkayi, M. B. Tagani, and H. R. Soleimani, *Chem. Phys. Lett*., **594**, 51 (2014). [DOI: https://doi.org/10.1016/j.cplett.2014.01.023]

[35] H. Shi, C. Liu, J. Xu, H. Song, B. Lu, F. Jiang, W. Zhou, G.

Zhang, and Q. Jiang, *ACS Appl. Mater. Interfaces*, **5**, 12811 (2013). [DOI: https://doi.org/10.1021/am404183v]

[36] H. Kang, L. Xu, Y. Cai, Y. Liu, F. Jiang, J. Xu, and W. Zhou, *Eur. Polym. J.*, **144**, 110208 (2021). [DOI: https://doi.org/10.1016/j.eurpolymj.2020.110208]

[37] X. Cao, M. Zhang, Y. Yang, H. Deng, and Q. Fu, *Compos. Commun.*, **27**, 100869 (2021). [DOI: https://doi.org/10.1016/j.coco.2021.100869]

[38] S. Xu, M. Hong, X. L. Shi, Y. Wang, L. Ge, Y. Bai, L. Wang, M. Dargusch, J. Zou, and Z. G. Chen, *Chem. Mater.*, **31**, 5238 (2019). [DOI: https://doi.org/10.1021/acs.chemmater.9b01500]

[39] Y. Wang, M. Hong, W. D. Liu, X. L. Shi, S. D. Xu, Q. Sun, H. Gao, S. Lu, J. Zou, and Z. G. Chen, *Chem. Eng. J.*, **397**, 125360 (2020). [DOI: https://doi.org/10.1016/j.cej.2020.125360]

[40] E. J. Bae, Y. H. Kang, C. Lee, and S. Y. Cho, *J. Mater. Chem. A*, **5**, 17867 (2017). [DOI: https://doi.org/10.1039/C7TA04280A]

[41] P. He, S. Shimano, K. Salikolimi, T. Isoshima, Y. Kakefuda, T. Mori, Y. Taguchi, Y. Ito, and M. Kawamoto, *ACS Appl. Mater. Interfaces*, **11**, 4211 (2018). [DOI: https://doi.org/10.1021/acsami.8b14820]

[42] Y. Hu, F. Jiang, B. Lu, C. Liu, J. Hou, and J. Xu, *Electrochim. Acta*, **228**, 361 (2017). [DOI: https://doi.org/10.1016/j.electacta.2017.01.019]

[43] W. Lee, C. T. Hong, O. H. Kwon, Y. Yoo, Y. H. Kang, J. Y. Lee, S. Y. Cho, and K. S. Jang, *ACS Appl. Mater. Interfaces*, **7**, 6550 (2015). [DOI: https://doi.org/10.1021/acsami.5b00626]

[44] E. Lim, K. A. Peterson, G. M. Su, and M. L. Chabinyc, *Chem. Mater.*, **30**, 998 (2018). [DOI: https://doi.org/10.1021/acs.chemmater.7b04849]

[45] J. Y. Kim, J. H. Jung, D. E. Lee, and J. Joo, *Synth. Met.*, **126**, 311 (2002). [DOI: https://doi.org/10.1016/S0379-6779(01)00576-8]

[46] G. H. Kim, L. Shao, K. Zhang, and K. P. Pipe, *Nat. Mater.*, **12**, 719 (2013). [DOI: https://doi.org/10.1038/nmat3635]

[47] J. Luo, D. Billep, T. Waechtler, T. Otto, M. Toader, O. Gordan, E. Sheremet, J. Martin, M. Hietschold, D.R.T. Zahn, and T. Gessner, *J. Mater. Chem. A*, **1**, 7576 (2013). [DOI: https://doi.org/10.1039/C3TA11209H]

[48] H. Ju and J. Kim, *ACS Nano*, **10**, 5730 (2016). [DOI: https://doi.org/10.1021/acsnano.5b07355]

[49] H. Ju, D. Park, and J. Kim, *Nanoscale*, **11**, 8502 (2019). [DOI: https://doi.org/10.1039/C9NR01345H].

[50] D. Park, M. Kim, and J. Kim, *Dalton Trans.*, **50**, 12424 (2021). [DOI: https://doi.org/10.1039/D1DT02297K]

[51] D. Park, M. Kim, and J. Kim, *Polymers*, **13**, 210 (2021). [DOI: https://doi.org/10.3390/polym13020210]

[52] Y. W. Park, Y. S. Lee, C. Park, L. W. Shacklette, and R. H. Baughman, *Solid State Commun.*, **63**, 1063 (1987). [DOI: https://doi.org/10.1016/0038-1098(87)90662-4]

[53] Y. W. Park, J. S. Moon, M. K. Bak, and J. I. Jin, *Synth. Met.*, **29**, 389 (1989). [DOI: https://doi.org/10.1016/0379-6779(89)90323-8]

[54] E. Dalas, S. Sakkopoulos, and E. Vitoratos, *J. Mater. Sci.*, **29**, 4131 (1994). [DOI: https://doi.org/10.1007/BF00355982]

[55] G. Prunet, F. Pawula, G. Fleury, E. Cloutet, A. J. Robinson, G. Hadziioannou, and A. Pakdel, *Mater. Today Phys.*, **18**, 100402 (2021). [DOI: https://doi.org/10.1016/j.mtphys.2021.100402]

[56] J. Li, X. Tang, H. Li, Y. Yan, and Q. Zhang, *Synth. Met.*, **160**, 1153 (2010). [DOI: https://doi.org/10.1016/j.synthmet.2010.03.001]

[57] C. Nath, A. Kumar, Y. K. Kuo, and G. S. Okram, *Appl. Phys. Lett.*, **105**, 133108 (2014). [DOI: https://doi.org/10.1063/1.4897146]

[58] H. Ju, D. Park, and J. Kim, *Polymer*, **160**, 24 (2019). [DOI: https://doi.org/10.1016/j.polymer.2018.11.036]

[59] M. Kuriakose, M. Depriester, R. Chan Yu King, F. Roussel, and A. Hadj Sahraoui, *J. Appl. Phys.*, **113**, 044502 (2013). [DOI: https://doi.org/10.1063/1.4788674]

[60] F. Roussel, R. Chan Yu King, M. Kuriakose, M. Depriester, A. Hadj-Sahraoui, C. Gors, A. Addad, and J. F. Brun, *Synth. Met.*, **199**, 196 (2015). [DOI: https://doi.org/10.1016/j.synthmet.2014.11.020]

[61] Y. Lu, Y. Song, and F. Wang, *Mater. Chem. Phys.*, **138**, 238 (2013). [DOI: https://doi.org/10.1016/j.matchemphys.2012.11.052]

[62] H. Ju, D. Park, and J. Kim, *Chem. Eng. J.*, **356**, 950 (2019). [DOI: https://doi.org/10.1016/j.cej.2018.09.106]

[63] H. Ju, D. Park, and J. Kim, *ACS Appl. Mater. Interfaces*, **10**, 11920 (2018). [DOI: https://doi.org/10.1021/acsami.7b19667]

[64] C. Dun, C. A. Hewitt, H. Huang, D. S. Montgomery, J. Xu, and D. L. Carroll, *Phys. Chem. Chem. Phys.*, **17**, 8591 (2015). [DOI: https://doi.org/10.1039/C4CP05390G]

[65] C. Dun, C. A. Hewitt, H. Huang, J. Xu, C. Zhou, W. Huang, Y. Cui, W. Zhou, Q. Jiang, and D. L. Carroll, *Nano Energy*, **18**, 306 (2015). [DOI: https://doi.org/10.1016/j.nanoen.2015.10.012]

[66] K. C. See, J. P. Feser, C. E. Chen, A. Majumdar, J. J. Urban, and R. A. Segalman, *Nano Lett.*, **10**, 4664 (2010). [DOI: https://doi.org/10.1021/nl102880k]

[67] Y. Wang, S. M. Zhang, and Y. Deng, *J. Mater. Chem. A*, **4**, 3554 (2016). [DOI: https://doi.org/10.1039/C6TA01140C]

[68] D. Park, M. Kim, and J. Kim, *J. Alloys Compd.*, **884**, 161098 (2021). [DOI: https://doi.org/10.1016/j.jallcom.2021.161098]

[69] Y. Lu, Y. Qiu, Q. Jiang, K. Cai, Y. Du, H. Song, M. Gao, C. Huang, J. He, and D. Hu, *ACS Appl. Mater. Interfaces*, **10**, 42310 (2018). [DOI: https://doi.org/10.1021/acsami.8b15252]

[70] Q. Meng, Q. Jiang, K. Cai, and L. Chen, *Org. Electron.*, **64**, 79 (2019). [DOI: https://doi.org/10.1016/j.orgel.2018.10.010]

[71] Y. Lu, Y. Ding, Y. Qiu, K. Cai, Q. Yao, H. Song, L. Tong, J. He, and L. Chen, *ACS Appl. Mater. Interfaces*, **11**, 12819 (2019). [DOI: https://doi.org/10.1021/acsami.9b01718]

[72] L. Wang, Z. Zhang, L. Geng, T. Yuan, Y. Liu, J. Guo, L. Fang, J. Qiu, and S. Wang, *Energy Environ. Sci.*, **11**, 1307 (2018). [DOI: https://doi.org/10.1039/C7EE03617E]